The human cytomegalovirus ER resident glycoprotein UL148 activates the unfolded protein response.

Mohammed N.A. Siddiquey,[a] Hongbo Zhang,[a] Christopher C. Nguyen,[a] Anthony J. Domma,[a] and Jeremy P. Kamil[a, #]

[a] Department of Microbiology and Immunology, LSU Health Sciences Center, Shreveport, Louisiana, U.S.A.

Running Head: HCMV UL148 activates the UPR

#Address correspondence to Jeremy P. Kamil, jkamil@lsuhsc.edu

ABSTRACT.

Eukaryotic cells are equipped with three sensors that respond to the accumulation of misfolded proteins within the lumen of the endoplasmic reticulum (ER) by activating the unfolded protein response (UPR), which functions to resolve proteotoxic stresses involving the secretory pathway. Here, we identify UL148, a viral ER resident glycoprotein from human cytomegalovirus (HCMV), as an inducer of the UPR. Metabolic labeling results indicate that global mRNA translation is markedly decreased when UL148 expression is induced in uninfected cells. Further, we find evidence suggesting that ectopic expression of UL148 is sufficient to activate at least two UPR sensors: the inositol requiring enzyme-1 (IRE1), as indicated by splicing of *Xbp1* mRNA, and the PKR-like ER kinase (PERK), as indicated by phosphorylation of eIF2α and accumulation of ATF4 protein. During wild-type HCMV infection, *Xbp-1* splicing, eIF2α phosphorylation and ATF4 accumulation neatly accompanied the onset of UL148 expression. However, the appearance of these UPR indicators was either markedly delayed or absent during *UL148*-null infections. siRNA depletion of PERK dampened the extent of eIF2α phosphorylation and ATF4 induction observed during wild-type infection, implicating PERK as opposed to other eIF2α kinases. A virus disrupted for *UL148* showed statistically significant 2- to 4-fold decreases during infection in the levels of transcripts canonically regulated by PERK/ATF4 and by the ATF6 pathway. Taken together, our results argue that UL148 is sufficient to activate the UPR when expressed ectopically and that UL148 is an important cause of UPR activation in the context of the HCMV infected cell.

IMPORTANCE.

The unfolded protein response (UPR) is an ancient cellular response to ER stress of broad importance to viruses. Certain consequences of the UPR, including mRNA degradation and translational shut-off, would presumably be disadvantageous to viruses, while other attributes of the UPR, such as ER expansion and upregulation of protein folding chaperones, might enhance viral replication. Although HCMV is estimated to express at least 200 distinct viral proteins, we show that the HCMV ER resident glycoprotein UL148 contributes substantially to the UPR during infection, and moreover is sufficient to activate the UPR in non-infected cells. Experimental activation of the UPR in mammalian cells is difficult to achieve without the use of toxins. Therefore, UL148 may provide a new tool to investigate fundamental aspects of the UPR. Furthermore, our findings may have implications for understanding the mechanisms underlying the effects of UL148 on HCMV cell tropism and evasion of cell mediated immunity.

INTRODUCTION

The endoplasmic reticulum (ER) is a fundamental eukaryotic organelle comprised of a tubulovesicular network of membranes that extends throughout the cytosol [reviewed in (1, 2)]. The organelle carries out multifarious processes vital to cellular and organismal health. For instance, the ER plays key roles in the regulation of intracellular calcium levels, and provides the site for steroid and lipid synthesis, loading of peptides onto MHC complexes (3), and synthesis and processing of proteins and protein complexes destined for secretion. Therefore, it is no surprise that the ER is exploited by a diverse array of viruses during their replication. For instance, polyomaviruses exploit the ER for entry (4, 5), whereas flaviviruses (6) and caliciviruses (7) remodel it to creates sites for replication. Large enveloped dsDNA viruses, such as those in the Herpesviridae, require the ER for the expression and processing of extraordinarily large amounts of viral glycoproteins needed for the assembly of progeny virions.

In order to utilize the ER to support their replication, however, viruses have had to develop mechanisms to contend with the unfolded protein response (UPR), an ancient stress response that serves to maintain ER function and cell viability when misfolded proteins accumulate within the secretory pathway [reviewed in (8, 9)]. The UPR is initiated by three different ER-based signaling molecules: inositol-requiring enzyme-1 (IRE1), the PKR-like ER kinase (PERK), and the cyclic AMP-dependent transcription factor 6 α (ATF6). Misfolded proteins are thought to displace the ER chaperone BiP (Grp78) from the luminal domains of IRE1, PERK and ATF6, which causes their activation. During the UPR, mRNA translation is attenuated, and

transcripts associated with rough ER ribosomes are degraded, and a number of genes are transcriptionally upregulated, resulting in increased expression of ER protein folding chaperones, ER-associated degradation (ERAD) proteins, as well as various factors that can expand the size and secretory capacity of the ER. Hence, certain consequences of the UPR, particularly translational attenuation, would be expected be deleterious to viruses, while others, such as ER expansion, could enhance the capacity of the infected host cell to produce progeny virions.

Cytomegaloviruses have been found to activate the UPR while subverting certain aspects of it (10, 11). Interestingly, the viral nuclear egress complex component m50 of murine cytomegalovirus (MCMV) degrades IRE1, and the human cytomegalovirus (HCMV) homolog UL50 apparently shares this activity (12). Cytoplasmic splicing of *Xbp-1* mRNA is mediated by IRE1 nuclease activity upon UPR activation. This splicing event is required for translation of the transcription factor XBP1s, which upregulates ERAD factors and ER chaperones, among other target genes (13). In addition, IRE1 degrades mRNAs undergoing translation at the rough ER (14). Therefore, IRE1 downregulation may help to maintain viral glycoprotein expression in the face of UPR activation. Despite this function of UL50, Isler et. al. found evidence that IRE1 is activated during HCMV infection (10). In addition to IRE1, PERK is activated during HCMV and MCMV infection (10, 11), and the PERK / ATF4 axis appears to be required for efficient viral replication, as defects in viral upregulation of lipid synthesis are observed in cells lacking PERK (15).

Interestingly, the viral proteins or processes that activate PERK and IRE1 in the context of HCMV infection have not been clearly identified. We recently reported that

UL148 interacts with SEL1L, a component of the cellular ERAD machinery that plays crucial roles in the disposal of misfolded proteins from the ER (16). Having observed very poor expression for any glycoprotein ectopically co-expressed with UL148 in uninfected cells (not shown), we hypothesized that UL148 might trigger the UPR. Here, we show that ectopically expressed UL148 is not only sufficient to activate the PERK and IRE1 arms of the UPR, but also strongly contributes to the activation of PERK and IRE1 during HCMV infection.

RESULTS

Ectopic expression of UL148 attenuates translation.

As a first step to formally investigate whether UL148 might contribute to ER stress that would trigger the unfolded protein response (UPR), we asked whether ectopic expression of UL148 in uninfected cells would dampen protein synthesis, since translational shutdown is a hallmark of stress responses, including the UPR. To address this question, we employed a “tet-on” lentiviral vector system that would allow us to inducibly express UL148 or its homolog from rhesus cytomegalovirus, Rh159 (17, 18), each harboring a C-terminal influenza A hemagluttinin (HA) epitope tag. Rh159 was used to control for any nonspecific effects of overexpression of an ER resident glycoprotein. We chose Rh159 as a control for the following reasons. Firstly, like UL148, Rh159 is predicted to be type I transmembrane protein with a very short cytoplasmic tail. Secondly, although Rh159 shares 30% amino acid identity with UL148, these two proteins appear to carry out different functions (18-20). Thirdly,

131 UL148 and Rh159 appeared to express at similar levels during ectopic expression (see
132 below).

133 Having isolated stably transduced ARPE-19 cell populations, we confirmed that
134 that anti-HA immunoreactive polypeptides of the expected size for UL148 ($i148^{HA}$) or
135 Rh159 ($i159^{HA}$) were induced upon treatment with 100 ng/mL doxycycline (dox) (Fig.
136 1A). Furthermore, expression of neither protein caused any overt reduction in cell
137 viability or number, as measured by trypan blue exclusion following 24 h of dox
138 induction (Fig. 1B, 1C). We therefore concluded that the $i148^{HA}$ and $i159^{HA}$ ARPE-19
139 cells were suitable to address whether UL148 might affect rates of mRNA translation in
140 metabolic labeling studies. For these experiments, $i148^{HA}$ and $i159^{HA}$ cells were induced
141 (or mock induced) for transgene expression for 24 h, and then incubated in the
142 presence of ^{35}S-labeled methionine and cysteine for 30 min. In parallel, labeling was
143 also carried out using $i159^{HA}$ cells that were incubated in the presence of either
144 thapsigargin (Tg) or carrier-alone, so as to provide positive and negative controls,
145 respectively, for UPR induction.

146 We found that expression of UL148 but not Rh159 caused a substantial, ~50%
147 decrease in protein synthesis compared to the carrier-alone (water) treated control, as
148 measured by phosphor-image analysis (Fig. 1D). Strikingly, the attenuation of
149 translation observed during UL148 expression was similar in magnitude to that seen
150 during Tg treatment (Fig. 1D). These effects did not appear to be caused by the
151 inducing agent, since dox treatment of $i159^{HA}$ cells failed to cause any reduction in ^{35}S
152 incorporation. From these results, we concluded that expression of UL148 attenuates
153 translation. Since UL148 is an ER resident glycoprotein, with a predicted type I

transmembrane topology that places most of the polypeptide in the ER lumen (19), it seemed plausible that the effects of UL148 on global rates of mRNA translation might be indicative of the UPR. We thus sought to address the hypothesis that UL148 activates the UPR.

UL148 leads to PERK-dependent phosphorylation of eIF2α and accumulation of ATF4.

Translational attenuation during the UPR is mediated by the PKR-like ER kinase, PERK, which phosphorylates Ser51 of the α-subunit of the ternary eIF2 complex (21). The guanine nucleotide exchange factor eIF2B binds to the phosphorylated eIF2 complex with increased affinity, and fails to exchange bound GDP for GTP (22). Since GDP/GTP exchange is necessary for eIF2 to participate in a new round of translational initiation, and because eIF2α is present in cells at a considerable molar excess relative to eIF2B, global protein synthesis halts in response to even modest levels of phosphorylated eIF2α [reviewed in (23)]. Meanwhile, eIF2α phosphorylation leads to enhanced translation of certain mRNAs, such as that encoding ATF4, which harbor μORFs in their 5'UTRs that inhibit their translation under non-stressed conditions (24). Although there are four different kinases that have been identified to phosphorylate eIF2α at Ser51, two observations imply that the translational attenuation we observed during UL148 expression was due to activation of PERK: (i) UL148 localizes to the ER (19), and (ii) interacts with the ERAD machinery (16). Therefore, we next monitored levels of PERK, eIF2α phosphorylation, and ATF4 following dox induction of either UL148 or Rh159 in ARPE-19 cells.

We observed that UL148 and Rh159 proteins accumulated to readily detectable levels by 8 h post induction with dox, although faint expression was detected at 4 h post induction (Fig. 2). By 24 h post induction, the i148^{HA} cells showed robust levels of ATF4 protein, albeit not as high as those seen during Tg treatment, which was included as a positive control for PERK activation. Increased levels of phospho-eIF2α were detected from 24 h to 48 h following induction of UL148, but not during induction of Rh159. Moreover, PERK protein levels appeared to be upregulated at 24 h post induction in i148^{HA} cells, but not in i159^{HA} cells. Decreased mobility of the anti-PERK immunoreactive band, which likely indicates PERK autophosphorylation upon UPR activation, was readily observed in the Tg condition, but not following induction of either UL148 or Rh159 (Fig. 2), which may indicate that PERK is less synchronously activated following dox-induction of UL148 than by the comparatively shorter (4 h) Tg treatment. Although we could not exclude the possibility that UL148 might cause these effects via activation of different eIF2α kinase, the simplest interpretation of these results is that expression of UL148 activates PERK.

UL148 is sufficient to induce splicing of *Xbp-1* mRNA.

To determine whether UL148 activates IRE1, we transfected human embryonic kidney (HEK)-293T cells with plasmids that drive expression of UL148 or Rh159 carrying C-terminal HA-tags. We also examined the effects of a 2 h treatment with 1 mM dithiothreitol (DTT), as a positive control treatment known to activate IRE1. At 48 h post transfection, we harvested cells for isolation of total RNA and for protein lysates to monitor transgene expression. As a read-out for IRE1 activity, we used reverse-

transcriptase PCR (RT-PCR) to detect the removal of 26 nucleotides (nt) from the *Xbp-1* mRNA. This unorthodox splicing event is catalyzed in the cytosol by IRE1; its detection is widely used as an indicator of the UPR in general, and of IRE1 nuclease activity in particular (25-27). Although we also tried this assay using our dox-inducible ARPE-19 cells (not shown), we found that transient transfection of HEK-293 cells gave the most readily interpretable results (Fig. 3).

As expected, the 2 h DTT treatment caused the 26-nt intron to be spliced from nearly all the *Xbp-1* mRNA detected in our assay (Fig. 3A). Cells transfected with either the Rh159 expression plasmid or empty vector failed to show notable levels of *Xbp-1* splicing. In contrast, removal of the 26-bp was readily detected from cells expressing UL148, with approximately equal levels of RT-PCR products for spliced and unspliced *Xbp-1* (Fig. 3A). Furthermore, the expression of anti-HA immunoreactive bands of the expected sizes for Rh159 and UL148 was confirmed by western blot (Fig. 3B). From these results, we concluded that ectopic expression of UL148 but not Rh159 is sufficient to induce splicing of the 26-nt intron from *Xbp-1* mRNA. Given that IRE1 is required for this splicing event (25-28), our results argue that UL148 expression is sufficient to activate IRE1.

UL148 activates IRE1 during HCMV infection.

Since UL148 was apparently capable of activating the UPR when ectopically expressed, we wondered whether UL148 might contribute to the UPR activation in the context of HCMV infection. Therefore, we conducted a time-course experiment comparing IRE1 catalyzed splicing of *Xbp-1* in fibroblasts infected at MOI 1 with either

wild-type (WT) HCMV strain TB40/E (TB_WT) or a *UL148*-null mutant, TB_148$_{STOP}$ (16). Remarkably, while WT infected cells showed increasing levels of spliced *Xbp-1* (*Xbp-1s*) as infection progressed, *UL148*-null virus infected cells, showed only very low levels of spliced *Xbp-1* that did not increase over time (Fig. 4). It is also notable that during WT infection the proportion of spliced to unspliced *Xbp-1* message increased from 24 hpi to 144 hpi. These effects correlate nicely with appearance of detectable levels of UL148 during infection and with increases in its levels that occur as infection progresses (Fig. 5). Further, we observed comparable levels of *IE2* mRNA by semi-quantitative RT-PCR, indicating that infection with the two viruses occurred at similar levels (Fig. 4). We interpreted these results to suggest that UL148 contributes to activation of IRE1 and concomitant cytoplasmic splicing of *Xbp-1* mRNA during HCMV infection. Since *Xbp-1* splicing is an important hallmark of UPR activation, these results also suggest that UL148 is a considerable source of ER stress in the context of HCMV infected cells.

UL148 contributes to PERK-dependent increases in phosphorylated eIF2α and ATF4 during HCMV infection.

To evaluate whether UL148 contributes to PERK activation during infection, we monitored levels of PERK, phospho-eIF2α, and ATF4 following MOI 1 infection of fibroblasts with WT or *UL148*-null virus. We found striking differences between the WT and *UL148*-disrupted infection contexts in each of these parameters, which together suggest a role for UL148 in activation of PERK. In WT infected cells, ATF4 levels showed an obvious increase at 48 h post infection (hpi) and reached near maximal expression at 72 hpi, with the highest levels detected at 96 hpi (Fig. 5A). The changes

246 in ATF4 expression during WT infection coincided with increased phosphorylation of
247 eIF2α and higher levels of PERK, as expected (10, 24). The kinetics of ATF4
248 expression tightly correlated, to a remarkable degree, with those seen for UL148 (Fig.
249 5A).

250 In cells infected with *UL148*-null virus, ATF4 was weakly expressed at most of
251 the time points monitored, although faint increases were seen at 72 hpi and 84 hpi. At
252 96 hpi, however, a strong burst of ATF4 expression was detected, which was
253 accompanied by an increase in phosphorylated eIF2α. This observation suggests that
254 UL148-independent activation of one or more eIF2α kinases occurs at very late times
255 during infection. Importantly, levels of the viral IE1 (IE1-72) protein were similar across
256 all time points for both viruses, indicating that infection occurred efficiently in both WT
257 and *UL148*-null settings (Fig. 5A), as would be expected since *UL148*-null mutants
258 replicate indistinguishably from WT in fibroblasts (19). Because the UL148-indepenent
259 rise in levels of phospho-eIF2α and ATF4 occurred between 84 and 96 hpi, we
260 reasoned that the 72 hpi time point would best allow us to isolate the effect of UL148 on
261 these indicators of PERK activation. By measuring the fluorescence signal from
262 secondary antibodies from multiple biological replicates, we were able to estimate that
263 at 72 hpi WT infected cells contain 2.5-fold higher levels of phospho-eIF2α, and 4.3-fold
264 higher levels of ATF4 relative to $UL148_{STOP}$ infections (Fig. 5B).

265 In order to more specifically address whether PERK is required for UL148 to
266 cause phosphorylation of eIF2α and accumulation of ATF4, we used siRNA to silence
267 PERK expression prior to infection, and then monitored for phosphorylation of eIF2α
268 and expression of ATF4 from 24 to 72 hpi. Levels of PERK were substantially reduced

but not completely eliminated by the PERK-targeted siRNA treatment, as compared to the non-targeting control siRNA (NTC) (Fig. 6). In PERK-silenced cells during WT infection, phosphorylation of eIF2α was attenuated at both 48 hpi and 72 hpi and a substantial decrease in ATF4 was seen at 72 hpi (Fig. 6). During *UL148*-null infections, however, PERK knockdown led to only minimal effects on phosphorylation of eIF2α, and virtually imperceptible effects on ATF4 (Fig. 6), which may well reflect reduced levels of ER stress in the absence of UL148.

Quantification of fluorescent secondary antibody signals suggested that in the case of WT virus at 72 hpi, PERK knockdown led to a 40% decrease in the levels of phospho-eIF2α and ATF4. Because the siRNA knockdown of PERK was incomplete, these results seem likely underestimate the degree to which UL148 depends on PERK to cause phosphorylation of eIF2α and to increase ATF4 expression. Overall, we interpreted these findings to argue that UL148 activates PERK during HCMV infection.

UL148 contributes to differences in mRNA levels for UPR target genes.

A major function of the UPR is to cause changes in cellular gene expression. Since ATF4 and XBP1s are transcription factors that contribute to UPR mediated changes in gene expression (13, 24, 29), we next wished to determine whether UL148 contributes to effects of HCMV on mRNA levels for cellular genes that are known to be regulated by the UPR. Further, because we were unable to obtain antibody sensitive enough to test whether activation of ATF6 was influenced by UL148 (not shown), and because it has been reported that HCMV infection does not lead to ATF6 activation, but that genes regulated by ATF6 are nonetheless upregulated (10, 30), we also sought to

address whether UL148 might contribute to upregulation of ATF6 target genes. Therefore, we isolated total RNA from WT and *UL148*-null infected fibroblasts at 72 hpi and used RT-qPCR to measure mRNA levels for representative UPR target genes, including ATF6 target genes in addition to those regulated by ATF4 (PERK) and XBP1s (IRE1).

With regard to the PERK pathway, our results show that relative to *UL148*-null virus infected cells, WT virus infected cells exhibited nearly 4-fold higher mRNA levels for the ATF4 target gene CHOP, and roughly 2-fold higher mRNA levels for another ATF4 target, GADD34 (Fig. 7). These differences were found to be statistically significant ($P<0.05$). Despite the UL148-dependent effects we observed on *Xbp-1* splicing (Figs. 3-4), the levels of mRNAs from XBP1s target genes did not appreciably differ between WT and *UL148*-null infections (Fig. 7). This result is consistent with a previous report that failed to find an effect of HCMV-induced *Xbp-1* splicing on mRNA levels for the XBP1s target gene *EDEM1* (10). Intriguingly, we did find significant differences for a number of ATF6 target genes that were upregulated in WT relative to *UL148*-null infections, including *BiP*, *SEL1L*, *HERPUD1*, and *HYOU1*, all of which showed approximately 2-fold higher expression during WT infection. Although *PDIA4* was upregulated by over two-fold in cells infected with WT virus compared to those infected with *UL148*-null virus, this difference was not found reach statistical significance. From these results, we concluded that UL148 contributes during HCMV infection to upregulation of UPR target genes related to the PERK and ATF6 arms of the UPR.

DISCUSSION

HCMV is estimated to encode 164-192 distinct genes (31, 32), with a more recent study arguing for up to 751 protein coding ORFs (33). Thus, the degree to which our results suggest that UL148 alone contributes to UPR induction during HCMV infection is remarkable. The original work demonstrating that HCMV activates the UPR conducted their studies using the laboratory-adapted virus strain Towne (10), which unlike another widely studied laboratory strain, AD169, retains the capacity to express UL148 (34, 35). Accordingly, the kinetics of ATF4 protein accumulation and phosphorylation of eIF2α that we observed for cells infected with wild-type (WT) strain TB40/E (Fig. 5) are highly consistent with those observed in the latter study (10), and the extent to which these indicators of PERK activation were dampened during *UL148*-null infection is striking (Figs. 5-6).

Cells infected with *UL148*-null viruses exhibited reduced levels of eIF2α phosphorylation and impaired induction of ATF4 at times prior to 96 hpi (Fig. 5). Although there are three other eIF2α kinases, we contend that because UL148 is an ER-resident protein, and also appears to activate IRE1, another sensor of ER stress, the effects on eIF2α phosphorylation and ATF4 levels most like occur via PERK. In support of this notion, PERK knockdown diminished the effect of UL148 on ATF4 induction (Fig. 6). Similarly, in studies with MCMV Qian et al. found that knockdown of PERK led to attenuated levels of ATF4 (11). Thus, both human and murine cytomegaloviruses appear to induce phosphorylation of eIF2α and ATF4 upregulation via PERK even though MCMV does not encode a UL148 homolog.

338 Furthermore, we detected 2 to 4-fold higher mRNA levels for two ATF4-regulated
339 regulated genes, CHOP and GADD34, in WT compared to *UL148*-null infected cells
340 (Fig. 7). As opposed to the effects of UL148 on *Xbp-1* splicing (Fig. 4), which were not
341 accompanied by differences in mRNA levels for XBP1s target genes, the effects of
342 UL148 on the PERK-ATF4 axis were accompanied by the expected changes in gene
343 expression (Fig. 6). Nonetheless, our *Xbp-1* splicing results argue that UL148 is
344 sufficient to activate IRE1 (Fig. 3). Moreover, UL148 appears to account for most of the
345 IRE1 activation observed during HCMV infection (Fig. 4). These effects are particularly
346 noteworthy as they presumably occur in the face of viral downregulation of IRE1 by the
347 viral nuclear egress factor UL50 (12).
348 Although the kinetics of *Xbp-1* splicing we observed during WT infection were
349 similar to those seen by Isler et al. (10), the ratio of spliced-to-unspliced message
350 appeared to be much higher in our results and may reflect differences in UL148
351 expression between strains Towne and TB40/E. In our hands, the Towne strain
352 appears to express UL148 at much lower levels than TB40/E (H. Zhang and J.P. Kamil,
353 unpublished results). Regardless, *XBP1s* target genes such as EDEM1 (36, 37) were
354 not found to be upregulated in a UL148-dependent manner (Fig. 6), as is fully consistent
355 with the findings of Isler et al. (10), who likewise failed to observe EDEM1 upregulation
356 despite observing *Xbp-1* splicing during infection.
357 Since XBP1s target genes are apparently refractory to IRE1 activation during
358 HCMV infection, the implications to the virus of IRE1 activation are unclear. However,
359 splicing of *Xbp-1* is not the only function of IRE1. IRE1 also activates the JNK signaling
360 pathway (38) and degrades mRNAs associated with the rough ER (14). Furthermore,

IRE1 confers resistance to apoptosis during hepatitis C infection by degrading mIR-125a (39). Albeit that we used *Xbp-1* splicing as a specific readout for activation of IRE1, it seems conceivable that functions of IRE1 unrelated to splicing of *Xbp-1* mRNA may be relevant to phenotypes governed by UL148.

Whether UL148 activates the third UPR sensor, ATF6, remains unresolved. *UL148*-null virus infected cells did show lower mRNA levels for ATF6 target genes compared to WT infected cells (Fig. 7), which may suggest that ATF6 is activated by UL148. Unfortunately, we have not been able to directly evaluate this matter directly, owing to the limited sensitivity in our hands of commercially available ATF6 antibodies (not shown). ATF6 is proteolytically processed by the same proteases that regulate sterol responsive element binding proteins (SREPBs), S1P and S2P (40). Under conditions of ER stress, ATF6 transits from the ER to the Golgi where S1P and S2P release the cytoplasmic domain of ATF6 from its transmembrane anchor, allowing it to transit to the nucleus where it binds to cis-acting ER stress regulatory elements (ERSE) and upregulates genes for ER chaperones, such as BiP (Grp78) (26, 41).

Nonetheless, upregulation of BiP reportedly occurs in an ERSE-independent manner during HCMV infection (30). Although Isler et al. were unable to detect ATF6 cleavage despite finding target genes to be upregulated during HCMV infection (10), the S1P/S2P processed nuclear form of ATF6, like SREBPs, is rapidly degraded in the absence of proteasome inhibitors (40). Hence, it is difficult to exclude the possibility that that low levels of ATF6 activation occur during HCMV infection. Given these circumstances, it may be challenging to address the potential role of UL148 in ATF6 activation.

Why would HCMV encode a protein that activates the UPR?

It is intriguing to consider why HCMV would encode a viral protein that potently triggers the UPR. *C*ertain consequences of the UPR, such as enhanced ERAD and attenuation of translation, might be expected to be unfavorable for viral replication. For instance, degradation of mRNAs by IRE1 could hamper the expression of viral glycoproteins, and phosphorylation of eIF2α by PERK could dampen viral gene expression. However, maintaining translation of viral mRNAs is a *sine qua non* for cytolytic viruses, and the literature resoundingly suggests HCMV is no exception [reviewed in (42)]. In particular, UL38 plays a role in disarming ER stress, as it appears to limit both PERK activation and stress-induced translation of *ATF4* mRNA during infection (43). Nonetheless, PERK is required for efficient HCMV replication, and defects in viral upregulation of lipid synthesis have been observed during infection of PERK depleted cells (15). Meanwhile, activation of ATF6 and IRE1 are required for ER expansion, upregulation of ER chaperones, and for increased synthesis of lipids (25, 41, 44-48), all of which may benefit viral replication.

Given the substantial contribution of UL148 to UPR activation documented here, and the potential for the UPR to both negatively and positively impact viral replication, it is puzzling that *UL148*-null viruses are found to replicate indistinguishably from WT virus in fibroblasts (16, 19). Although we cannot yet exclude whether decreased induction of the UPR contributes to the enhanced growth of *UL148*-null virus in epithelial cells, the influence of UL148 on the expression of alternative gH/gL complexes, particularly gH/gL/gO, (16, 19) seems a more likely explanation. A derivative of the HCMV strain

AD169 that was restored both for *UL148* and for expression of the pentameric gH/gL/UL128-131 complex (16) appears to replicate at least as well in epithelial cells as the parental virus lacking *UL148*, while failing to show differences in gH/gL/gO expression in virions (Nguyen C.C., Siddiquey, M.N.A., Li, G. and Kamil J.P., unpublished results). We thus consider it unlikely that expression of UL148 is directly detrimental to productive replication of HCMV in epithelial cells, especially since viral factors such as UL50 (12) and UL38 (43, 49) would be expected to blunt any negative impacts to the virus of UPR induction.

Implications for mechanisms underlying *UL148* dependent phenotypes.

Going forward, it will be crucial to delineate which biological roles and/or phenotypic effects of UL148 require induction of the UPR. We cannot yet dismiss the possibility that UPR induction is incidental to the *bona fide* biological function(s) of UL148, which could be modulation of virion cell tropism (19), or evasion of cell-mediated immune responses (20). In other words, UPR activation may not be required for the effects of UL148 that provide a fitness advantage to the virus. For example, although the HCMV ER resident immune-ëvasin US11 triggers the UPR in uninfected cells, the UPR does not appear to be required for US11-mediated degradation of the MHC I heavy chain (50). On the other hand, certain observations suggest that UPR induction may be inseparable from the role of UL148 in cell tropism. We recently reported that UL148 co-purifies from infected cells with SEL1L, a key component of the cellular machinery for ER associated degradation (ERAD) , and have found that UL148 attenuates ERAD of newly synthesized glycoprotein O (gO), which itself appears to be a

constitutive substrate for ERAD (16). Therefore, one might hypothesize that UL148 interacts with the ERAD machinery to impede processing of misfolded proteins, which consequently results in UPR activation.

UL148 was recently found to block surface presentation of CD58 (LFA3), a co-stimulatory ligand that potentiates T-lymphocyte and NK-cell responses (20). Intriguingly, UL148 causes markedly reduced N-glycosylation of CD58 (20), which is exactly the opposite of its effect on gO (16, 19). Rh159, which shares significant sequence homology with UL148 and is involved in retention of a distinct set of co-stimulatory molecules(18), does not appear to activate the UPR (Figs. 1-3). Although it is unknown whether UL148 requires UPR activation to downregulate CD58, knowledge of the proximal events by which UL148 activates the UPR will likely prove integral to understanding the mechanisms underlying its influence on viral immune evasion and modulation of tropism.

Finally, it is worth pointing out that UL148 may hold promise as a reagent to investigate the UPR itself. Much of our understanding of the mammalian UPR comes from experimental approaches in which toxic chemicals, such as thapsigargin or tunicamycin, are relied upon to synchronously and robustly induce the UPR in cultured cells. A recent report found that such chemicals fail to accurately recapitulate the authentic UPR induced by unfolded proteins within the ER lumen (51). Albeit that the molecular events by which UL148 initiates the UPR remain to be determined, this viral ER resident glycoprotein may represent a fascinating new tool to interrogate how cells adapt to ER stress.

MATERIALS AND METHODS.

Cells and Virus.

Primary Human foreskin fibroblasts (HFF, ATCC #SCRC-1041) were immortalized by transducing lentivirus encoding human telomerase (hTERT) to yield HFFT cells. HEK-293T cells were purchased from Genhunter Corp. (Nashville, TN). The retinal pigment epithelial cell line ARPE-19 was purchased from ATCC (CRL-2302). All cells were cultured in Dulbecco's Modified Eagle's Medium (DMEM, Corning # 10013CV) supplemented with 25 µg/mL gentamicin, 10 µg/mL ciprofloxacin-HCl, and either 5% fetal bovine serum (FBS, Sigma-Aldrich #F2442) or 5% newborn calf serum (NCS, Sigma-Aldrich #N4637).

Viruses were reconstituted by electroporation of HCMV bacterial artificial chromosomes (BACs) into HFFTs, as described previously (19, 52), and grown until 100% CPE was observed. Cell-associated virus was released by Dounce-homogenization of pelleted infected cells, clarified of cell debris by centrifugation (1000*g*, 10 min), and combined with the culture supernatants. Cell-associated and cell-free virus containing virus were combined and then ultracentrifuged through a 20% sorbitol cushion (85,000*g*, 1 h, 4˚C). The resulting virus pellet was resuspended in DMEM containing 20% NCS. Viruses for this study were all derived from the bacterial artificial chromosome clone of HCMV strain TB40/E, TB40E-BAC4 (53), which was a generous gift of Christian Sinzger (Ulm, Germany). A *UL148*- null mutant derived from TB40E-BAC4, TB_148$_{STOP}$, has been described elsewhere (16). BACs and plasmid DNAs for transfection were purified from *E. coli* using Nucleobond Xtra Midi kits (Machery-Nagel, Inc.).

476

477 **Virus titration.**

478 Infectivity of virus stocks and samples were determined by the tissue culture infectious
479 dose 50% ($TCID_{50}$) assay. Briefly, serial dilutions of virus were used to infect multiple
480 wells of a 96-well plate. After 9 days, wells were scored as positive or negative for CPE,
481 and $TCID_{50}$ values were calculated according to the Spearman-Kärber method, as
482 described previously (16).

483

484 **Construction of plasmids.**

485 UL148 and Rh159 were PCR amplified from plasmids pEF1-UL148HA (19) and pcDNA-
486 Rh159 IRES-GFP (a gift of Klaus Frueh, Oregon Health Sciences University, Beaverton,
487 OR) using primer pairs UL148_reclone_Fw and UL148 reclone Rv, and Rh159 Fw and
488 Rh159_HA_Rv, respectively (Table 1). The PCR product for UL148 was ligated into
489 pcDNA3.1(+) (Invitrogen) using the BamHI and EcoRI sites, while the PCR product for
490 Rh159 was inserted into the EcoRV site using a Gibson Assembly Reaction using NEB
491 HiFi DNA assembly Master Mix (New England Biolabs). Final plasmids were sequence
492 confirmed using T7 and BGH reverse primers. To construct lentiviral vectors for inducible
493 expression of Rh159 and UL148, pInducer10-miR-RUP-PheS (54) (a generous gift of
494 Stephen J. Elledge, Harvard Medical School, Addgene #44011) was digested with NotI
495 and MluI to remove the miR-30 cassette and re-assembled using oligo RFP_stitch in
496 Gibson reaction (55) to yield pIND-RFP. Plasmid pTRE3G-dTomato was assembled by
497 Vector Builder. The TRE3G promoter was PCR-amplified with primers TRE3Gvb_Fw and
498 TRE3Gvb_Rv and assembled into EcoRV-digested pSP72 by Gibson reaction to yield

499 pSP72-TRE3G, which was sequence-verified using universal primer SP6. Following the
500 example of Stinski and coworkers (56), the *crs* of the minimal CMV promoter within
501 TRE3G was mutated from CGTTTAGTGAACCGT to CAGGTAGTGAACCGT by overlap
502 extension PCR using primers TRE3G_crsmut_Fw and TRE3G_crsmut_Rv (57). Finally,
503 the Δ*crs* TRE3G promoter was digested out of pSP72-TRE3G using NheI/AgeI and
504 ligated into NheI/AgeI-digested pIND-RFP to yield pOUPc-RFP. pOUPc-UL148HA was
505 constructed by PCR amplifying the UL148HA CDS from plasmid pcDNA3.1-UL148HA
506 using primers UL148HAgibs_Fw and HAgibs_Rv and Gibson-assembling the product into
507 AgeI/MluI-digested pOUPc-RFP. pOUPc-Rh159HA was constructed by PCR amplifying
508 the Rh159HA CDS from plasmid pcDNA3.1-Rh159HA using primers Rh159HAgibs_Fw
509 and HAeco_gibs_Rv and Gibson-assembling the product into AgeI/MluI-digested pOUPc-
510 RFP. pOUPc-UL148HA and -Rh159HA were sequence-confirmed using primers
511 CMVcrsnull_Fw and Ubc_Rv.
512
513 **Lentivirus vector transduction.** To generate stable i148^{HA} and i159^{HA} cell populations,
514 replication defective HIV-1 based lentivirus vector particles were generated from pOUPc-
515 UL148HA or -Rh159HA, as described previously (52). Briefly, 5 × 10^5 293T cells per well
516 of a six-well cluster plate were co-transfected with pOUPc-UL148HA or pOUPc -
517 Rh159HA, together with psPAX2 (Addgene #12260) and pMD2.G (Addgene #12259)
518 using *Trans*IT-293 reagent (Mirus Bio, Inc.) as per the manufacturer's instructions.
519 Supernatants collected at 2 and 3 d post-transfection were combined, filtered through a
520 0.45 µm cellulose acetate syringe filter (Corning, Inc.), added to complete DMEM growth
521 medium supplemented with 8 µg/mL polybrene (Sigma Aldrich) and applied to

522 subconfluent ARPE-19 monolayers. The next day, medium was removed and the cells
523 were washed three times with Dulbecco's PBS (PBS: 2.7 mM KCl, 1.5 mM KH_2PO_4, 137
524 mM NaCl, 8.1 mM Na_2HPO_4, pH 7.4). Starting at 2 d post-transduction, cells were
525 serially-passaged in medium containing 2 µg/mL puromycin HCl until resistant cells grew
526 out.
527
528 **Metabolic labeling.** $i159^{HA}$ or $i148^{HA}$ cells were seeded at 2×10^5 cells per well in a 24-
529 well cluster plate in Gibco OptiMEM reduced serum medium (Thermo Fisher)
530 supplemented with 2.5% tetracycline (tet)-free FBS (Clontech #631101). The following
531 day, medium was replaced with 2.5% tet-free FBS OptiMEM supplemented with either
532 100 ng/mL doxycycline hyclate (dox, Sigma Aldrich #D9891, added from a 1000× stock)
533 or the addition of 0.1% (vol/vol) of sterile water to control for volume of dox stock solution
534 (mock induction). At 24 h post-induction, cells were washed twice in PBS supplemented
535 with 1 mM $CaCl_2$ and 0.5 mM $MgCl_2$ and then incubated for 1 h in starving medium
536 (DMEM lacking methionie, cysteine, and glutamine, (Gibco #21013024, supplemented
537 with 5% dialyzed FBS, Sigma #F0392, and 2 mM glutamine). Cells were then pulse-
538 labeled in starving medium containing 150 µCi/mL ^{35}S-Met/Cys (PerkinElmer #NEG772)
539 for 30 min. Dox or mock treatment was maintained throughout the starving and pulsing
540 steps. As a positive control for translation shutdown, $i159^{HA}$ ARPE19 cells were treated
541 with 2 µM thapsigargin (Sigma #T9033) or 0.1% dimethyl-sulfoxide (DMSO) as a carrier-
542 control at 1 h prior to Met/Cys starvation, and treatment was maintained throughout the
543 starvation and pulse-labeling steps. Following pulse-labeling, cells were washed three
544 times in PBS containing 1 mM $CaCl_2$ and 0.5 mM $MgCl_2$, and then immediately lysed in

2 × Laemmli buffer [120 mM Tris pH 6.8, 4% SDS, 20% glycerol, 0.02% bromophenol blue]. Beta-mercaptoethanol was then added to a final concentration of 5% vol/vol, and the samples were heated at 95˚C for 10 min. Equal volumes of lysate were resolved by sodium dodecyl sulfate polyacrylamide gel electrophoresis (SDS-PAGE) on 12% acrylamide NuPAGE Bis-Tris precast gels (Invitrogen #NP0321) according to manufacturer's instructions. Gels were dried and exposed to a phosphor screen for 24 h before results were captured using an Amersham Typhoon IP scanner (GE Heathcare). Relative signal per lane was calculated using Bio-Rad 1-D analysis software by reading the signal volume (counts*mm^2) in each lane. Lane signals were normalized either to (i) the DMSO treatment condition or (ii) each respective non-treatment condition.

Cell viability assay

1 × 10^5 i148^{HA} or i159^{HA} ARPE-19 cells per well were seeded in a 24 well cluster plate and incubated overnight. Medium was exchanged for complete DMEM containing 100 ng/mL doxycycline and incubated for 24 h. Cells were then trypsinized, transferred to 1.5 mL microfuge tubes and spun down at 400 × *g* for 5 min. Cell pellets were resuspended in 100 µL fresh medium and combined with 100 µL of PBS containing 0.4% Trypan Blue (Bio-Rad), mixed thoroughly and counted for viability (trypan blue exclusion) and total cell number using a hematocytometer (Bright-Line).

Doxycycline induction of UL148 and Rh159 from stably transduced ARPE-19 cells.

For each well of a 24 well cluster plate, 2 × 10^5 cells of iUL148 or iRh159 ARPE19 cells were seeded in 500 µl OptiMEM medium containing 2.5% tetracycline(tet)-free FBS

(Clontech #631101). Following a 24 h incubation at 37^{0}C, medium was replaced with fresh 2.5% tet-free FBS/OptiMEM supplemented with 100 ng/mL doxycycline hyclate (dox, Sigma Aldrich #9891). Where indicated, parallel wells of ARPE-19 cells were incubated for 4 h in the presence of 200 nM thapsigargin (Tg) prior to harvest. At the indicated times post treatment, cells were washed in PBS and lysed for 1 h at 4˚C using 50 µl per well of lysis buffer (1% Triton X-100, 400 mM NaCl, 0.5% sodium deoxycholate, 50 mM HEPES pH 7.5) supplemented with 1 × protease inhibitor cocktail (Cell Signaling Technology). Lysates were collected and spun down at 18,000 × *g* for 30 min at 4˚C. Protein concentrations of supernatants were measured using the BCA assay (Thermo Pierce), normalized, and subjected to western blot.

siRNA treatments.

2 × 10^5 HFFTs per well of a 24-well plate were reverse transfected with 5 pmol per well of a Dharmacon siGENOME SMARTpool specific for human PERK (EIF2AK3, M004883-03-005) or with a non-targeting control SMARTpool (D-001206-14-05), using 4.5 µL of Lipofectamine RNAiMAX per well, as described previously (16). Briefly, siRNA transfection complexes in OptiMEM medium were added to wells prior to applying freshly trypsinized HFFT suspended in 0.45 mL of DMEM containing 8% FBS, 25 µg/mL gentamicin, and 10 µg/mL ciprofloxacin-HCl. 24 h post-seeding, cells were infected with the indicated viruses at an MOI of 1 $TCID_{50}$ per cell. Sequences of the siRNAs in each SMARTpool are provided in Table 2.

Xbp-1 splicing assay.

591 HEK-293T cells were seeded into 24-well plates for overnight culture and transfected
592 once they reached 80-90% confluency using the TransIT 2020 reagent (Mirus, Inc.), with
593 each well receiving 1 µg plasmid DNA carried by 3 µL of the transfection reagent. 48 h
594 post transfection, cells were harvested and total RNA was extracted using the Qiagen
595 RNeasy mini kit as per the manufacturer's protocol, including the optional column
596 DNAase digestion step. cDNA was generated from 1 µg RNA using the qScript™ cDNA
597 Synthesis Kit (Quantabio, Cat# 95047-100) in a 20 µL final reaction volume. One
598 microliter of the resulting cDNA solution was then used as template for a PCR reaction
599 using primers Xbp-1_FWD and Xbp-1_REV (Table 1). In the context of infection (Fig. 4),
600 detection of *IE2* (*UL122*) mRNA was included as indicator of HCMV infection. The *IE2*
601 primer pair was designed using PrimerQuest software (Integrated DNA Technologies,
602 Coralville, IA), and includes one oligonucleotide whose priming site spans the junction of
603 exons 3 and 5 (Table 1).
604
605 **Quantitative reverse-transcriptase PCR.**
606 mRNA levels were quantified using reverse-transcriptase qPCR (RT-qPCR). For these
607 experiments, 2×10^6 HFFT cells per well were seeded in a 6 well cluster plate, incubated
608 overnight and subsequently infected at MOI 1. At 24 hpi, inocula were removed and
609 replaced with fresh medium. At 72 hpi, total RNA was extracted using a Qiagen RNeasy
610 Mini Kit (Qiagen, Inc.), including the optional on-column DNase digestion step, as per the
611 manufacturer's instructions. cDNA was generated from 1 µg RNA using the qScript™
612 cDNA synthesis kit. For each qPCR reaction, 1 µl of cDNA was used as template in a
613 15 µL final reaction volume using iQ SYBR Green Supermix (Bio-Rad, Inc.) on a CFX96

614 Real Time PCR system (Bio-Rad). mRNA levels for each gene were measured in
615 triplicate technical replicates per biological replicate, with a total of three independent
616 biological replicates, and the $2^{-\Delta\Delta C_T}$ method (58) was used to determine quantitative
617 estimates of relative gene expression, with all readings being normalized to *GAPDH*
618 transcript levels. Canonical UPR responsive target genes were detected using previously
619 validated qPCR primer pairs (29, 59), while levels of the viral *IE1 (UL123)* mRNA were
620 also measured as an indicator of HCMV infection (Table 1). PCR efficiencies for primer
621 pairs ranged from 91.1% - 99.0% for the indicated UPR target genes and were 93.4% for
622 *GAPDH* and 90.7% for *IE1*. Statistical Analyses were done using GraphPad Prism
623 software, version 6.0h (GraphPad, Inc., La Jolla, CA).

624

625 **Antibodies used in this study**

626 The following rabbit monoclonal antibodies (mAbs) from Cell Signaling Technology,
627 (Danvers, MA) were used: ATF4 clone D4B8 (cat. #11815S), PERK clone C33E10 (cat.
628 #3192S), Phospho-eIF2α Ser51 clone D9G8 (cat. #3398S), total eIF2α clone D7D3 (cat.
629 #5324S). IE1 was detected using mouse mAb clone1B12 (Gift of Thomas Shenk,
630 Princeton University), beta-actin using a rabbit mAb, (Li-Cor Biosciences, Inc.; cat. #926-
631 42210), a rabbit polyclonal anti-HA epitope antibody (Bethyl Laboratories, Inc.,
632 Montgomery, TX), and a previously described rabbit polyclonal serum specific for UL148
633 (19).

634 **Western blotting**

635 For detection of all proteins other than phospho-Ser51 eIF2α (see below), western blotting
636 was carried out as previously described (16, 19, 52). Briefly, cells were lysed at 4˚C for
637 1 h in lysis buffer [1% Triton X-100, 400 mM NaCl, 0.5% sodium deoxycholate, 50 mM 4-
638 (2-hydroxyethyl)-1-piperazineethanesulfonic acid (HEPES) pH 7.5 supplemented with 1
639 × protease inhibitor cocktail (Cell Signaling Technology)]. Lysates were clarified by
640 centrifugation at 18,000 × *g* for 30 min at 4˚C, combined with an equal volume of 2 ×
641 Laemmli buffer containing 10% betamercaptoethanol, heated at 85˚C for 10 min prior to
642 being resolved by SDS-PAGE on 10% acrylamide gels and transferred to nitrocellulose
643 membranes (Whatman Protran®, 0.45 µm pore size). Efficient transfer was confirmed
644 using Ponceau S staining (not shown). All subsequent blocking, washes, and incubation
645 steps were performed with gentle rocking. Membranes were blocked using a solution of
646 5% powdered milk (PM) in PBS containing 0.01% Tween-20 (PBST), (PM-PBST). Unless
647 otherwise noted, all antibodies were applied to membranes in PM-PBST, as a 1:1000
648 dilution, or for IE1 mAb, a 1:200 dilution of the hybridoma supernatant, and incubated
649 overnight 4˚C, or for 1 h at room temperature. Following three 5 min washes in 1 × PBS,
650 IRDye-800 conjugated donkey anti-rabbit or anti-mouse secondary antibodies (Li-Cor,
651 Inc.) were applied at 1:10,000 in PM-PBST and incubated for 1 h. After 3 washes in
652 PBST, immunoreactive polypeptides were detected, and where applicable, quantified
653 using a Li-Cor Odyssey Imager (Li-Cor Biosciences). For detection of Ser51
654 phosphorylated eIF2α, a protocol from the laboratory of David Ron (Cambridge Institute
655 for Medical Research, United Kingdom) was used. The differences from our standard
656 procedures were as follows: Membranes were blocked for 2 h at room temperature in a
657 solution of 5% bovine serum albumin (BSA) in PBS containing 0.01% Tween-20, followed

658 by a second 10 min blocking step in PM-PBST. Following three washes in PBS,
659 membranes were incubated overnight in a solution of phospho-eIF2α antibody diluted
660 1:1000 in PBS supplemented with 5% BSA.
661

662 **ACKNOWLEDGMENTS**

663 This project was supported by NIH Grants R01-AI116851 and P30GM110703. Its
664 contents are solely the responsibility of the authors and do not necessarily represent the
665 official views of the NIAID or the NIGMS. C.C.N. was supported by a Malcolm Feist
666 Predoctoral Fellowship from the Center of Cardiovascular Diseases and Sciences at
667 LSU Health Sciences Center, Shreveport. We are grateful to Thomas Shenk (Princeton
668 University, Princeton, NJ, USA), Christian Sinzger (University of Ulm Medical Center,
669 Ulm, Germany), and Klaus Früh (Oregon Health Sciences University, Beaverton, OR,
670 USA) for generously providing reagents.

671

672

673 **FIGURES.**

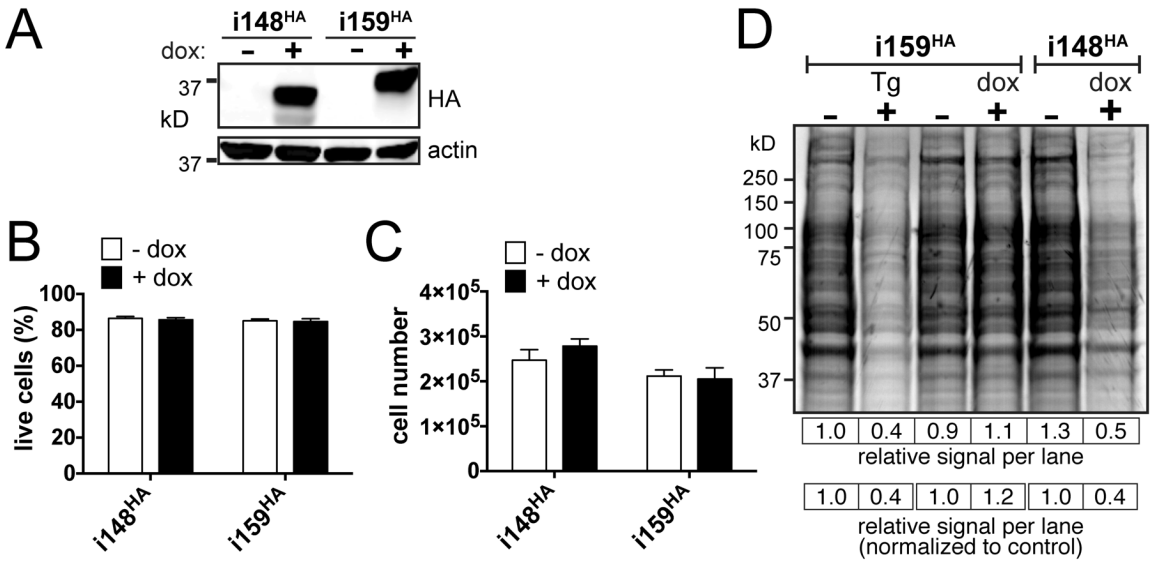

674

675 **FIGURE 1. Ectopic expression of UL148 attenuates translation**
676 **(A)** Validation of expression system: i148^{HA} and i159^{HA} ARPE-19 cells were treated with
677 either 100 ng/mL doxycycline (dox) or carrier-alone (water) and subjected to western
678 blot using anti-HA antibodies; beta-actin (actin) was detected as a loading control. **(B)**
679 and **(C)** UL148 expression does not have overtly toxic effects: i148^{HA} and i159^{HA}
680 ARPE-19 cells were dox- or mock induced for 24 h. Viable cells from triplicate
681 treatments were scored using trypan blue exclusion and total cell number on a
682 hematocytometer. **(D)** i148^{HA} and i159^{HA} cells were either dox induced or mock treated
683 (0.1% water) for 24 h, and in parallel, additional wells of i159^{HA} cells were treated for 2 h
684 with either 2 μM thapsigargin (Tg) or 0.1% DMSO carrier-alone. Cells were then pulsed
685 with ^{35}S methionine +cysteine for 30 min, and protein lysates were resolved by SDS-
686 PAGE and imaged by autoradiography. Quantitation of the total signal intensity per
687 lane is shown relative to that of the (-) Tg lane (leftmost) directly below the gel image
688 and for each treatment lane relative to its paired negative control.
689

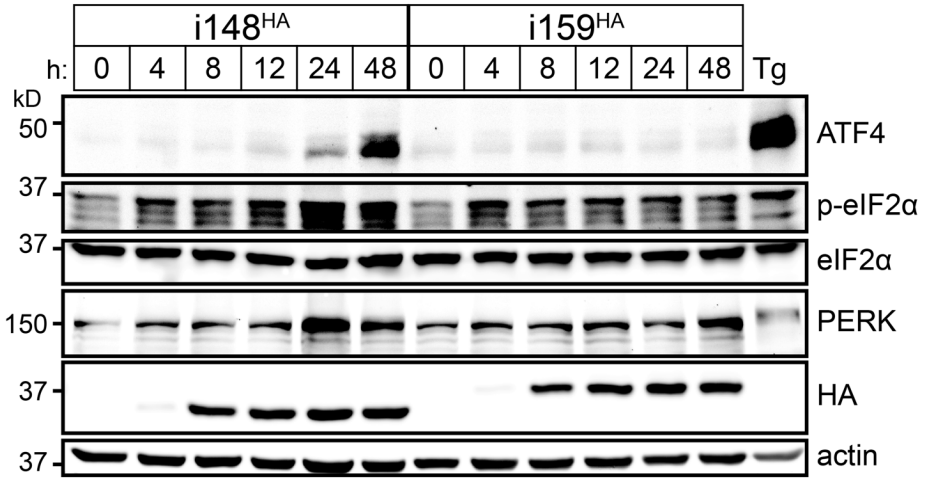

FIGURE. 2. UL148 expression causes phosphorylation of eIF2α and accumulation of ATF4, suggesting activation of PERK

i148^{HA} and i159^{HA} ARPE-19 cells were induced for expression of UL148 and Rh159, respectively, using 100 ng/mL doxycycline (dox) for the indicated times. A 4 h treatment with thapsigargin (Tg) (0.4 μM) was included as positive control. For each sample, a volume of lysate equivalent to 17.5 μg of detergent soluble protein was analyzed by western blot for levels of the indicated proteins.

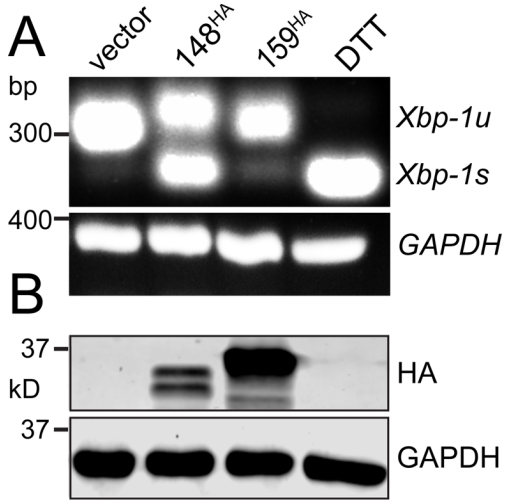

FIGURE 3. UL148 induces splicing of *Xbp-1* mRNA

HEK-293T cells were transfected with 1 µg of plasmid DNA for the indicated expression constructs or with empty vector as a negative control. **(A)** 48 h post transfection, total RNA was isolated and used in an RT-PCR assay to detect removal of the 26 nt intron from *Xbp-1* mRNA. *Xbp-1s*: spliced message, *Xbp-1u*: unspliced message. A 2 h treatment with dithiothreitol (DTT, 1 mM) was used as positive control. **(B)** UL148 and Rh159 were detected using anti-HA western blot. In both panels, *gapdh* mRNA or GAPDH protein was detected as a loading control.

712

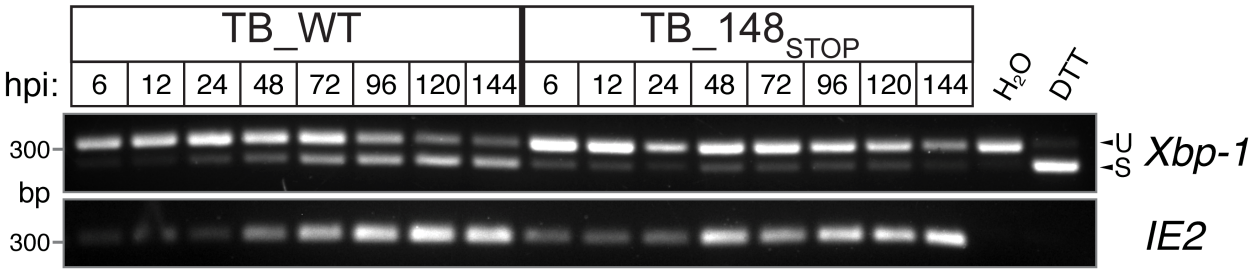

713

714 **FIGURE 4. UL148 activates IRE1 during HCMV infection.**
715 Fibroblasts were infected MOI of 1 $TCID_{50}$ per cell with wild-type HCMV strain TB40/E,
716 (TB_WT) or a *UL148*-null mutant virus, (TB _148_{STOP}). At the indicated times post
717 infection, total RNA was harvested and subjected to RT-PCR to detect IRE1 catalyzed
718 removal of the 26 bp intron from the *Xbp-1* mRNA. Semi-quantitative RT-PCR of *IE2*
719 (*UL122*) is shown as a control to indicate HCMV gene expression. U: unspliced, S:
720 spliced. DTT: dithiothreitol, a positive control.
721

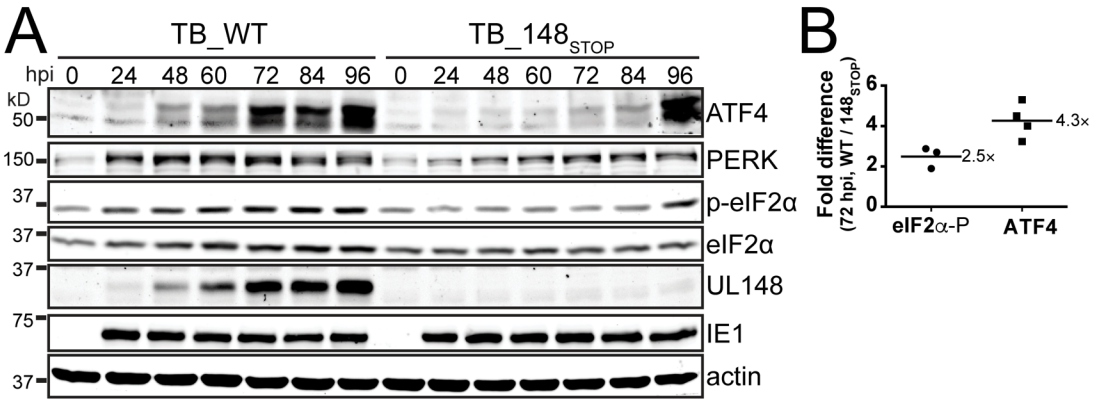

FIGURE 5. UL148 is required for increases in eIF2α phosphorylation and ATF4 protein expression during HCMV infection.

(A) Fibroblasts were infected MOI of 1 $TCID_{50}$ per cell with TB_WT or TB_148_{STOP} viruses for the indicated times and subsequently assayed by western blot (25 µg of protein per lane) for levels of ATF4, PERK, p-eIF2α, eIF2α, UL148, IE1, and beta-actin. **(B)** Fold-difference in phospho-eIF2α (p-eIF2α) and ATF4 protein signals at 72 hpi between TB_WT or TB_148_{STOP}. Fluorescence signal from secondary antibodies at the 72 hpi time points was quantified from western blots comparing TB_WT and TB_148_{STOP} infections, as in (**A**), using three independent biological replicates for p-eIF2α and four biological replicates for ATF4.

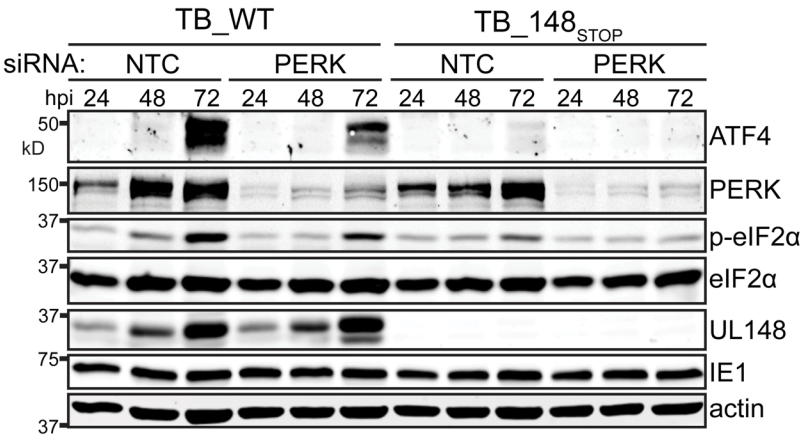

FIGURE 6. PERK contributes to the effects of UL148 on eIF2α phosphorylation and ATF4 protein levels.

Fibroblasts were reverse-transfected using an siRNA SMARTpool targeting PERK or a non-targeting control siRNA pool (NTC). 24 h later, the cells were infected at an MOI of1 $TCID_{50}$ per cell with either TB_WT or TB_148_{STOP} viruses for the indicated times. Cell lysates were assayed by immunoblot for expression of the indicated proteins.

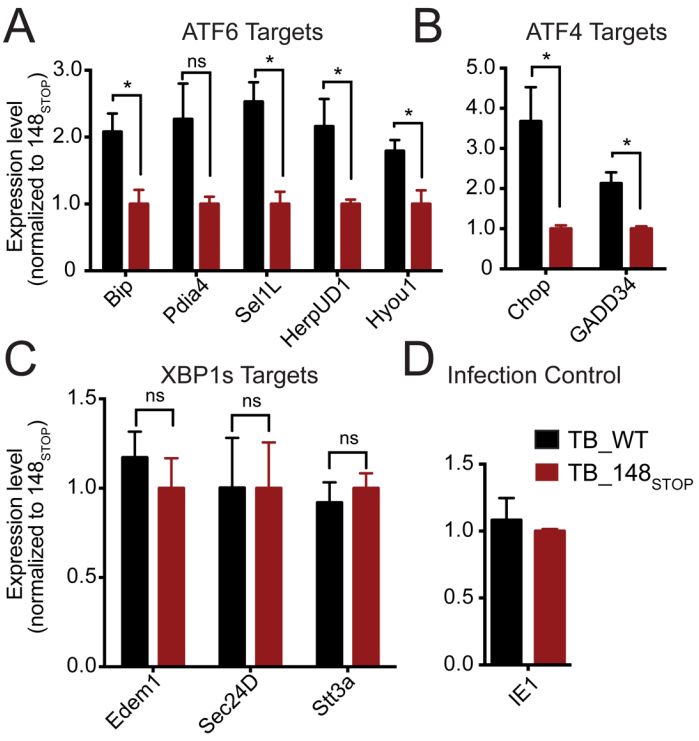

743

744 **FIGURE 7. Analysis of mRNA levels for UPR target genes during WT and *UL148*-**
745 **null infection**. Fibroblasts were infected at an MOI of 1 $TCID_{50}$ per cell with TB_WT or
746 TB_148_{STOP} viruses. At 72 h post infection, mRNA levels for the indicated genes were
747 analyzed by quantitative RT-PCR. Asterisks indicate differences found to be
748 statistically significant in a two-tailed T-test ($P<0.05$).
749

750

751 **REFERENCES**

752

753 1. Lin JH, Walter P, Yen TS. 2008. Endoplasmic reticulum stress in disease
754 pathogenesis. Annu Rev Pathol 3:399-425.
755 2. Voeltz GK, Rolls MM, Rapoport TA. 2002. Structural organization of the endoplasmic
756 reticulum. EMBO Rep 3:944-50.
757 3. Kleijmeer MJ, Kelly A, Geuze HJ, Slot JW, Townsend A, Trowsdale J. 1992. Location of
758 MHC-encoded transporters in the endoplasmic reticulum and cis-Golgi. Nature
759 357:342-4.
760 4. Kartenbeck J, Stukenbrok H, Helenius A. 1989. Endocytosis of simian virus 40 into
761 the endoplasmic reticulum. J Cell Biol 109:2721-9.
762 5. Tsai B, Gilbert JM, Stehle T, Lencer W, Benjamin TL, Rapoport TA. 2003. Gangliosides
763 are receptors for murine polyoma virus and SV40. EMBO J 22:4346-55.
764 6. Gillespie LK, Hoenen A, Morgan G, Mackenzie JM. 2010. The endoplasmic reticulum
765 provides the membrane platform for biogenesis of the flavivirus replication
766 complex. J Virol 84:10438-47.
767 7. Bailey D, Kaiser WJ, Hollinshead M, Moffat K, Chaudhry Y, Wileman T, Sosnovtsev SV,
768 Goodfellow IG. 2010. Feline calicivirus p32, p39 and p30 proteins localize to the
769 endoplasmic reticulum to initiate replication complex formation. J Gen Virol 91:739-
770 49.
771 8. Ron D, Walter P. 2007. Signal integration in the endoplasmic reticulum unfolded
772 protein response. Nat Rev Mol Cell Biol 8:519-29.
773 9. Walter P, Ron D. 2011. The unfolded protein response: from stress pathway to
774 homeostatic regulation. Science 334:1081-6.
775 10. Isler JA, Skalet AH, Alwine JC. 2005. Human cytomegalovirus infection activates and
776 regulates the unfolded protein response. J Virol 79:6890-9.
777 11. Qian Z, Xuan B, Chapa TJ, Gualberto N, Yu D. 2012. Murine cytomegalovirus targets
778 transcription factor ATF4 to exploit the unfolded-protein response. J Virol 86:6712-
779 23.
780 12. Stahl S, Burkhart JM, Hinte F, Tirosh B, Mohr H, Zahedi RP, Sickmann A, Ruzsics Z,
781 Budt M, Brune W. 2013. Cytomegalovirus downregulates IRE1 to repress the
782 unfolded protein response. PLoS Pathog 9:e1003544.
783 13. Lee AH, Iwakoshi NN, Glimcher LH. 2003. XBP-1 regulates a subset of endoplasmic
784 reticulum resident chaperone genes in the unfolded protein response. Mol Cell Biol
785 23:7448-59.
786 14. Hollien J, Lin JH, Li H, Stevens N, Walter P, Weissman JS. 2009. Regulated Ire1-
787 dependent decay of messenger RNAs in mammalian cells. J Cell Biol 186:323-31.
788 15. Yu Y, Pierciey FJ, Jr., Maguire TG, Alwine JC. 2013. PKR-like endoplasmic reticulum
789 kinase is necessary for lipogenic activation during HCMV infection. PLoS Pathog
790 9:e1003266.
791 16. Nguyen C, Siddiquey MNA, Zhang H, Kamil JP. 2018. Human cytomegalovirus
792 tropism modulator UL148 interacts with SEL1L, a cellular factor that governs ER-
793 associated degradation of the viral envelope glycoprotein, gO.
794 bioRxiv:https://doi.org/10.1101/304394.

17. Lilja AE, Chang WL, Barry PA, Becerra SP, Shenk TE. 2008. Functional genetic analysis of rhesus cytomegalovirus: Rh01 is an epithelial cell tropism factor. J Virol 82:2170-81.
18. Sturgill ER, Malouli D, Hansen SG, Burwitz BJ, Seo S, Schneider CL, Womack JL, Verweij MC, Ventura AB, Bhusari A, Jeffries KM, Legasse AW, Axthelm MK, Hudson AW, Sacha JB, Picker LJ, Fruh K. 2016. Natural Killer Cell Evasion Is Essential for Infection by Rhesus Cytomegalovirus. PLoS Pathog 12:e1005868.
19. Li G, Nguyen CC, Ryckman BJ, Britt WJ, Kamil JP. 2015. A viral regulator of glycoprotein complexes contributes to human cytomegalovirus cell tropism. Proc Natl Acad Sci U S A 112:4471-6.
20. Wang ECY, Pjechova M, Nightingale K, Vlahava VM, Patel M, Ruckova E, Forbes SK, Nobre L, Antrobus R, Roberts D, Fielding CA, Seirafian S, Davies J, Murrell I, Lau B, Wilkie GS, Suarez NM, Stanton RJ, Vojtesek B, Davison A, Lehner PJ, Weekes MP, Wilkinson GWG, Tomasec P. 2018. Suppression of costimulation by human cytomegalovirus promotes evasion of cellular immune defenses. Proc Natl Acad Sci U S A 115:4998-5003.
21. Harding HP, Zhang Y, Ron D. 1999. Protein translation and folding are coupled by an endoplasmic-reticulum-resident kinase. Nature 397:271-4.
22. Pavitt GD, Ramaiah KV, Kimball SR, Hinnebusch AG. 1998. eIF2 independently binds two distinct eIF2B subcomplexes that catalyze and regulate guanine-nucleotide exchange. Genes Dev 12:514-26.
23. Proud CG. 2005. eIF2 and the control of cell physiology. Semin Cell Dev Biol 16:3-12.
24. Harding HP, Novoa I, Zhang Y, Zeng H, Wek R, Schapira M, Ron D. 2000. Regulated translation initiation controls stress-induced gene expression in mammalian cells. Mol Cell 6:1099-108.
25. Calfon M, Zeng H, Urano F, Till JH, Hubbard SR, Harding HP, Clark SG, Ron D. 2002. IRE1 couples endoplasmic reticulum load to secretory capacity by processing the XBP-1 mRNA. Nature 415:92-6.
26. Lee K, Tirasophon W, Shen X, Michalak M, Prywes R, Okada T, Yoshida H, Mori K, Kaufman RJ. 2002. IRE1-mediated unconventional mRNA splicing and S2P-mediated ATF6 cleavage merge to regulate XBP1 in signaling the unfolded protein response. Genes Dev 16:452-66.
27. Yoshida H, Matsui T, Yamamoto A, Okada T, Mori K. 2001. XBP1 mRNA is induced by ATF6 and spliced by IRE1 in response to ER stress to produce a highly active transcription factor. Cell 107:881-91.
28. Sidrauski C, Walter P. 1997. The transmembrane kinase Ire1p is a site-specific endonuclease that initiates mRNA splicing in the unfolded protein response. Cell 90:1031-9.
29. Shoulders MD, Ryno LM, Genereux JC, Moresco JJ, Tu PG, Wu C, Yates JR, 3rd, Su AI, Kelly JW, Wiseman RL. 2013. Stress-independent activation of XBP1s and/or ATF6 reveals three functionally diverse ER proteostasis environments. Cell Rep 3:1279-92.
30. Buchkovich NJ, Yu Y, Pierciey FJ, Jr., Alwine JC. 2010. Human cytomegalovirus induces the endoplasmic reticulum chaperone BiP through increased transcription and activation of translation by using the BiP internal ribosome entry site. J Virol 84:11479-86.

31. Davison AJ, Dolan A, Akter P, Addison C, Dargan DJ, Alcendor DJ, McGeoch DJ, Hayward GS. 2003. The human cytomegalovirus genome revisited: comparison with the chimpanzee cytomegalovirus genome. J Gen Virol 84:17-28.
32. Murphy E, Rigoutsos I, Shibuya T, Shenk TE. 2003. Reevaluation of human cytomegalovirus coding potential. Proc Natl Acad Sci U S A 100:13585-90.
33. Stern-Ginossar N, Weisburd B, Michalski A, Le VT, Hein MY, Huang SX, Ma M, Shen B, Qian SB, Hengel H, Mann M, Ingolia NT, Weissman JS. 2012. Decoding human cytomegalovirus. Science 338:1088-93.
34. Cha TA, Tom E, Kemble GW, Duke GM, Mocarski ES, Spaete RR. 1996. Human cytomegalovirus clinical isolates carry at least 19 genes not found in laboratory strains. J Virol 70:78-83.
35. Dunn W, Chou C, Li H, Hai R, Patterson D, Stolc V, Zhu H, Liu F. 2003. Functional profiling of a human cytomegalovirus genome. Proc Natl Acad Sci U S A 100:14223-8.
36. Yoshida H, Matsui T, Hosokawa N, Kaufman RJ, Nagata K, Mori K. 2003. A time-dependent phase shift in the mammalian unfolded protein response. Dev Cell 4:265-71.
37. Yoshida H, Oku M, Suzuki M, Mori K. 2006. pXBP1(U) encoded in XBP1 pre-mRNA negatively regulates unfolded protein response activator pXBP1(S) in mammalian ER stress response. J Cell Biol 172:565-75.
38. Urano F, Wang X, Bertolotti A, Zhang Y, Chung P, Harding HP, Ron D. 2000. Coupling of stress in the ER to activation of JNK protein kinases by transmembrane protein kinase IRE1. Science 287:664-6.
39. Fink SL, Jayewickreme TR, Molony RD, Iwawaki T, Landis CS, Lindenbach BD, Iwasaki A. 2017. IRE1alpha promotes viral infection by conferring resistance to apoptosis. Sci Signal 10.
40. Ye J, Rawson RB, Komuro R, Chen X, Dave UP, Prywes R, Brown MS, Goldstein JL. 2000. ER stress induces cleavage of membrane-bound ATF6 by the same proteases that process SREBPs. Mol Cell 6:1355-64.
41. Yoshida H, Haze K, Yanagi H, Yura T, Mori K. 1998. Identification of the cis-acting endoplasmic reticulum stress response element responsible for transcriptional induction of mammalian glucose-regulated proteins. Involvement of basic leucine zipper transcription factors. J Biol Chem 273:33741-9.
42. Vincent HA, Ziehr B, Moorman NJ. 2016. Human Cytomegalovirus Strategies to Maintain and Promote mRNA Translation. Viruses 8:97.
43. Xuan B, Qian Z, Torigoi E, Yu D. 2009. Human cytomegalovirus protein pUL38 induces ATF4 expression, inhibits persistent JNK phosphorylation, and suppresses endoplasmic reticulum stress-induced cell death. J Virol 83:3463-74.
44. Sriburi R, Jackowski S, Mori K, Brewer JW. 2004. XBP1: a link between the unfolded protein response, lipid biosynthesis, and biogenesis of the endoplasmic reticulum. J Cell Biol 167:35-41.
45. Roy B, Lee AS. 1999. The mammalian endoplasmic reticulum stress response element consists of an evolutionarily conserved tripartite structure and interacts with a novel stress-inducible complex. Nucleic Acids Res 27:1437-43.

46. Maiuolo J, Bulotta S, Verderio C, Benfante R, Borgese N. 2011. Selective activation of the transcription factor ATF6 mediates endoplasmic reticulum proliferation triggered by a membrane protein. Proc Natl Acad Sci U S A 108:7832-7.
47. Cox JS, Chapman RE, Walter P. 1997. The unfolded protein response coordinates the production of endoplasmic reticulum protein and endoplasmic reticulum membrane. Mol Biol Cell 8:1805-14.
48. Reimold AM, Iwakoshi NN, Manis J, Vallabhajosyula P, Szomolanyi-Tsuda E, Gravallese EM, Friend D, Grusby MJ, Alt F, Glimcher LH. 2001. Plasma cell differentiation requires the transcription factor XBP-1. Nature 412:300-7.
49. Qian Z, Xuan B, Gualberto N, Yu D. 2011. The human cytomegalovirus protein pUL38 suppresses endoplasmic reticulum stress-mediated cell death independently of its ability to induce mTORC1 activation. J Virol 85:9103-13.
50. Tirosh B, Iwakoshi NN, Lilley BN, Lee AH, Glimcher LH, Ploegh HL. 2005. Human cytomegalovirus protein US11 provokes an unfolded protein response that may facilitate the degradation of class I major histocompatibility complex products. J Virol 79:2768-79.
51. Bergmann TJ, Fregno I, Fumagalli F, Rinaldi A, Bertoni F, Boersema PJ, Picotti P, Molinari M. 2018. Chemical stresses fail to mimic the unfolded protein response resulting from luminal load with unfolded polypeptides. J Biol Chem 293:5600-5612.
52. Wang D, Li G, Schauflinger M, Nguyen CC, Hall ED, Yurochko AD, von Einem J, Kamil JP. 2013. The ULb' region of the human cytomegalovirus genome confers an increased requirement for the viral protein kinase UL97. J Virol 87:6359-76.
53. Sinzger C, Hahn G, Digel M, Katona R, Sampaio KL, Messerle M, Hengel H, Koszinowski U, Brune W, Adler B. 2008. Cloning and sequencing of a highly productive, endotheliotropic virus strain derived from human cytomegalovirus TB40/E. J Gen Virol 89:359-68.
54. Meerbrey KL, Hu G, Kessler JD, Roarty K, Li MZ, Fang JE, Herschkowitz JI, Burrows AE, Ciccia A, Sun T, Schmitt EM, Bernardi RJ, Fu X, Bland CS, Cooper TA, Schiff R, Rosen JM, Westbrook TF, Elledge SJ. 2011. The pINDUCER lentiviral toolkit for inducible RNA interference in vitro and in vivo. Proc Natl Acad Sci U S A 108:3665-70.
55. Gibson DG, Smith HO, Hutchison CA, 3rd, Venter JC, Merryman C. 2010. Chemical synthesis of the mouse mitochondrial genome. Nat Methods 7:901-3.
56. Macias MP, Huang L, Lashmit PE, Stinski MF. 1996. Cellular or viral protein binding to a cytomegalovirus promoter transcription initiation site: effects on transcription. J Virol 70:3628-35.
57. Ho SN, Hunt HD, Horton RM, Pullen JK, Pease LR. 1989. Site-directed mutagenesis by overlap extension using the polymerase chain reaction. Gene 77:51-9.
58. Livak KJ, Schmittgen TD. 2001. Analysis of relative gene expression data using real-time quantitative PCR and the 2(-Delta Delta C(T)) Method. Methods 25:402-8.
59. van Galen P, Kreso A, Mbong N, Kent DG, Fitzmaurice T, Chambers JE, Xie S, Laurenti E, Hermans K, Eppert K, Marciniak SJ, Goodall JC, Green AR, Wouters BG, Wienholds E, Dick JE. 2014. The unfolded protein response governs integrity of the haematopoietic stem-cell pool during stress. Nature 510:268-72.